AIAA SciTech Forum
8-12 January 2024, Orlando, FL
AIAA SCITECH 2024 Forum

10.2514/6.2024-1988

Qualitative Analysis of Variable Speed Proportional Navigation Guidance Law

Nobin Paul* and Debasish Ghose†
Indian Institute of Science, Bangalore, 560012, India

This paper provides a comprehensive analysis of the performance of variable speed pure proportional navigation (PPN) guidance law. Although capturability analysis of constant speed proportional navigation guidance law has been addressed by researchers, the engagement equations involved are highly nonlinear and solving them is a complex procedure, often resulting in complex functions. In the literature, a qualitative analysis technique is commonly employed to determine the capture conditions for the constant speed PPN guidance law without actually solving the equations of motion. However, in the case of varying interceptor velocity, which this paper addresses, has remained an open problem. In this paper a qualitative approach is used to determine the capture conditions of a variable speed interceptor which uses PPN to generate lateral acceleration commands to achieve interception. The paper utilizes a velocity variation method that encompasses switching between different velocity values, allowing for the identification of capture conditions that account for both abrupt and gradual velocity changes.

I. Introduction

In this paper, we present a qualitative analysis of the capturability of the proportional navigation (PN) guidance law for time-varying interceptor speeds against a non-maneuvering but moving target. In the literature, captuarbility analysis of PN guidance law has been presented for constant speeds, stationary targets, and variable lateral acceleration bounds but not for time-varying speeds. The case of time-varying speed is a very important aspect of PN guidance, as most interceptors exhibit speed variations that are mostly dependent on largely uncontrollable factors such as drag, propulsion characteristics, etc. From this point of view, this paper makes a significant contribution not just in theoretical capturability analysis but also because it addresses a practically relevant scenario and departs from the simplistic assumption of constant velocity models.

Proportional navigation (PN) guidance law and its variants have been studied extensively in the literature. It is the most frequently used guidance law due to its computational simplicity, effectiveness, robustness, and ease of implementation [1]. PN guidance was first introduced in the literature by Yuan [2], and was extensively studied and implemented in tactical interceptors by Hughes aircraft company [3]. A linearized interceptor–target engagement geometry is introduced in [4]. Since closed-form solutions for PPN nonlinear equations for relative motions are difficult to obtain, a qualitative analysis to determine the capture conditions for the PPN guidance law was introduced in [5], which discusses the qualitative study of proportional navigation against non-maneuvering targets. Subsequently, a similar analysis was also done for maneuvering targets in [6, 7] to determine a set of sufficient conditions for which the interceptor can capture a target undergoing constant target maneuvers. Becker [8] discussed a closed-form solution of the PPN nonlinear equations of motion for an interceptor pursuing a non-maneuvering target using the methods from the theory of complex functions and obtaining the sufficient conditions for interception. In [9], the qualitative analysis method was extended to the capturability analysis of PPN against maneuvering target with a time-varying normal acceleration. A Lyapunov function technique is used in [10] for time-varying target maneuvers considering two-dimensional space. An extension of the Lyapunov approach to the three-dimensional space is given in [11, 12]. A qualitative analysis of augmented pure proportional navigation (APN) is also discussed in [13]. Besides APN, several other guidance laws were also derived to account for target lateral acceleration. Some of them had PN-based formulations [14], whereas others were based on optimal control [15] and game-theoretic problem formulation [16, 17]. A survey of many traditional and modern guidance laws are available in [18, 19].

Several guidance laws have been proposed to intercept moving targets. However, most of them do not investigate the impact of the interceptor's longitudinal acceleration on the trajectory. One exception is the TPN guidance law, where the longitudinal acceleration is applied not by design but by virtue of the interceptor acceleration being at an arbitrary angle

*Research Scholar, Guidance, Control and Decision Systems Laboratory, Department of Aerospace Engineering
†Professor, RBCCPS and Guidance, Control and Decision Systems Laboratory, Department of Aerospace Engineering

to its velocity vector. In addition to TPN, several approaches were applied to address the interceptor's variable speed in guidance problems. A standard solution to the variable-speed guidance problem is presented in [20] by adding an acceleration compensation term to the LOS rate in the guidance law. In [21], a generalized proportional navigation law is used to generate lateral acceleration commands to minimize the effect of the interceptor and target's constant longitudinal acceleration and guide the interceptor toward the target. In [22], an approximate guidance law with a modified APPN is considered to achieve interception during the boost and decelerating phases of the interceptor. In [23–25], the authors analyze the collision course for a variable-speed interceptor and define a guidance law that steers the heading of the interceptor to the collision course based on optimal control and differential game formulations. In [26], the authors establish an optimal guidance law for an interceptor with a time-varying guidance gain and time-varying time-to-go that accounts for the effect of the interceptor's future velocity changes. A time-varying linear pursuit–evasion game model with bounded controls is presented for the interceptor, and the target having variable speeds and lateral acceleration limits in [27, 28]. In [29], optimal guidance-to-collision guidance law was developed specifically for an exo-atmospheric interception scenario between an accelerating interceptor and a constant-speed target. In [30], interception of stationary targets by interceptors with arbitrary time-varying velocity is considered. A speed control-based guidance concept is presented in [31]. In [32], an optimal interceptor guidance law is used for target interception while imposing a predetermined terminal intercept angle with varying interceptor and target speeds. In [33], a linear quadratic guidance law with intercept angle constraints is used for varying speed adversaries. The performance of PPN-guided interceptors with arbitrary time-varying speed against stationary targets is explained in [34]. A guidance system with separate impact point prediction, specifically to deal with time-varying speeds of interceptors and target and a guidance law for generating the steering command to nullify the heading error is proposed in [35]. In [31, 36], a new guidance strategy is proposed in which variable speed is used as a guidance command, and it entirely ignores lateral acceleration as a steering mechanism. In [37], a mathematical analysis of the capturability of PPN guidance law, when the missile-to-target range fluctuates with time due to target maneuver, was presented for constant speed interceptor and a similar capturability analysis was extended in [38] for variable speed interceptors. In [39], a qualitative study of post-launch capturability of a PN guidance law was discussed for the interceptor, where the interceptor and the target have lateral and longitudinal accelerations. But it considered the engagement from a favourable initial condition for interception. In [40], in our prior work, we introduced a longitudinal acceleration-based variable speed (LAVS) guidance law which commands both lateral acceleration and longitudinal acceleration. Lateral acceleration command is generated from conventional PN guidance law, and longitudinal acceleration is given by a new method inspired by hawk's attack [41].

Even though most of the variable speed guidance laws described above use PN or its variants, there is no capturability analysis for PN guidance law with time-varying speeds for moving targets available in the literature. This paper presents a qualitative analysis of variable speed PN guidance law against a non-maneuvering but moving target.

This paper is organized as follows: Section II discusses the problem formulation and preliminary analysis. Section III covers the qualitative analysis of the relative velocity equations. Section IV examines different capture conditions for the variable speed PPN guidance law when applied to non-maneuvering targets. Finally, Section V outlines the conclusions and potential future works as extensions of this work.

II. Problem Formulation and Preliminary Analysis

Consider the engagement geometry in the plane, as shown in Fig. (1). Point mass models of target T and interceptor M are considered with velocities V_M and V_T. Here, R is the distance from the interceptor to the target, θ is the line of sight angle, α_M is the heading angle of the interceptor, and A_M is the lateral acceleration of the interceptor.

The equations of the relative motion between the interceptor and the target can be written as

$$V_R = V_T \cos\theta - V_M \cos(\alpha_M - \theta) \tag{1}$$

$$V_\theta = -V_T \sin\theta - V_M \sin(\alpha_M - \theta) \tag{2}$$

The lateral acceleration of the pursuer defined by PN guidance law, and the heading angle rate can be represented as

$$\dot{\alpha_M} = N\dot{\theta} \tag{3}$$

where N is the navigation constant, $\dot{\theta}$ line of sight angle rate, $\dot{\alpha_M}$ heading angle rate, and the lateral acceleration command is given by

$$A_M = NV_M\dot{\theta} \tag{4}$$

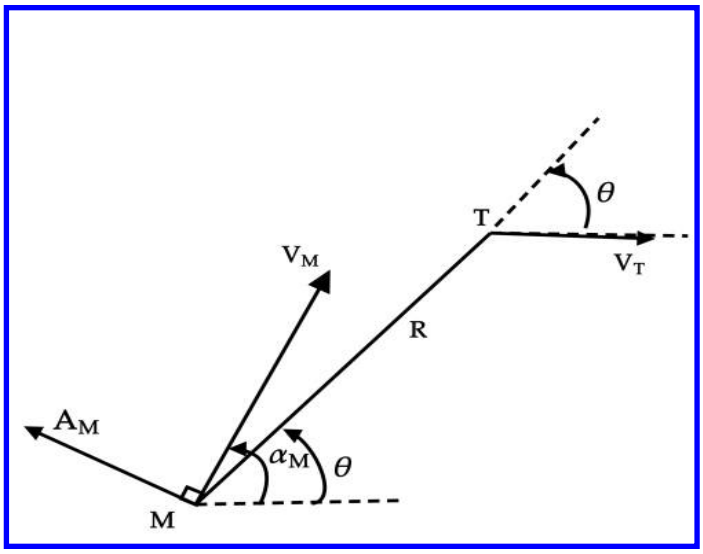

Fig. 1 Engagement geometry

Integrating Eqn. (3), we will get

$$\alpha_M - \alpha_{M0} = N(\theta - \theta_0) \tag{5}$$

where α_{M0} is the initial heading angle, and θ_0 is the initial line of sight angle. Consider

$$k = N - 1 \tag{6}$$

and

$$\phi_0 = -N\theta_0 + \alpha_{M0} \tag{7}$$

where k and ϕ_0 are constants that depend on the initial conditions and parameters. Substituting these constants in Eqn. (5), we will get

$$\alpha_M - \theta = k\theta + \phi_0 \tag{8}$$

Let $\nu = \frac{V_M}{V_T}$ define the velocity ratio, which will be subject to changes as the interceptor speed varies with time. Substituting Eqn. (8) in Eqns. (1), and (2), and considering the fact that ν is varying throughout the engagement, relative motion equations can be written as

$$V_R(\theta, \nu) = \cos\theta - \nu\cos(k\theta + \phi_0) \tag{9}$$

$$V_\theta(\theta, \nu) = -\sin\theta - \nu\sin(k\theta + \phi_0) \tag{10}$$

The above equations align with the formulation given in [5]. However, in the proposed formulation, we assume that the velocity ratio ν can vary between two bounds given by $\nu \in [\nu_{\min}, \nu_{\max}]$. Note that this variation can happen not only because the interceptor speed varies but may also happen due to the varying speed of the target, or both.

III. Qualitative Analysis

This section presents a qualitative analysis to determine the conditions for a successful capture by an interceptor against a non-maneuvering target. The engagement equations are nonlinear; hence, obtaining a closed-form analytical solution is challenging. This analysis assumes that the interceptor's speed is greater than that of the target during the engagement. The roots of the Eqns (9) and (10) are θ_R and θ_θ, respectively. The following lemmas can be defined for a constant ν.

Lemma 1. For any given $\nu\epsilon[\nu_{\min}, \nu_{\max}]$, if $\nu > 1$ and $k\nu > 1$ the roots of the equations $V_R(\theta, \nu) = 0$ and $V_\theta(\theta, \nu) = 0$ alternate along θ axis.

Lemma 2. For any given $\nu\epsilon[\nu_{\min}, \nu_{\max}]$, if $\nu > 1$ and $k\nu > 1$,

$$V_R(\theta_\theta)\frac{dV_\theta}{dt}(\theta_\theta) > 0 \tag{11}$$

where θ_θ is the roots of $V_\theta(\theta, \nu) = 0$

These lemmas were proved in [5] for a fixed value of ν. Since we assume the value of ν also to be fixed within the given bound, the same lemmas still hold. However, since ν can have different values in this paper, we need a somewhat more generalized analysis and modified results. Consider that the ν axis is normal to the plane of the paper with (V_θ,θ) and (V_R,θ) are two axes in the plane. The graph between V_θ or V_R, θ, and ν can be represented by a manifold when plotted. We will now show that if we select any plane parallel to (V_θ, θ) or (V_R, θ) plane we will get the curves for a particular $\nu\epsilon[\nu_{\min}, \nu_{\max}]$. If we project all the curves to (V_θ, θ) and (V_R, θ) plane for all ν, the roots of V_θ and V_R passes through some bands on the θ axis.

Fig. 2 shows the plots V_θ $vs.$ θ and V_R $vs.$ θ for $\nu\epsilon[\nu_{\min}, \nu_{\max}]$. The bands shown are the values of θ for which V_θ (or V_R) become zero for some value of θ for $\nu\epsilon[\nu_{\min}, \nu_{\max}]$. The bands are numbered by superscripts $i-1$, i, $i+1$, $i+2$, $i+3$ and subscripts θ, and R where, θ and R denote that these are the roots of V_θ and V_R, respectively. In addition, we also denote the boundaries of these bands by $\nu_{\min}$ and $\nu_{\max}$, implying that these boundaries correspond to the minimum and maximum values of ν. Note that, although there is a definite lower bound on ν ($\nu > 1$, given by Lemma 1 and 2), there is no fixed upper bound, implying that $\nu_{\max}$ can be very large indeed. To represent this fact we also show a boundary on the bands at $\nu = \infty$. The boundaries on θ for these bands are represented by θ with superscripts $i-1$, i, $i+1$, $i+2$, $i+3$ which represent the band number and subscripts θ, and R where, θ and R denote that these are the roots of V_θ and V_R, respectively. In addition, the specified and $\nu = \infty$ represent that the specified θ, as shown, corresponds to the ν for $\nu_{\min}$, $\nu_{\max}$, and $\nu = \infty$, respectively.

Our analysis identified two distinct categories of bands of θ, which are obtained when ν changes. The first category exhibits an increasing trend in θ_θ or θ_R as ν increases from $\nu_{\min}$ to $\nu_{\max}$, whereas the second category shows an opposite behavior, with θ_θ or θ_R decreasing as ν increases from $\nu_{\min}$ to $\nu_{\max}$. In Fig. 2, θ_θ is decreasing when ν increases in $\theta_\theta^{band\, i-1}$ and $\theta_\theta^{band\, i}$ and θ_θ is increasing when ν increases in $\theta_\theta^{band\, i+1}$ and $\theta_\theta^{band\, i+2}$. Similar behaviour also can be noticed for bands in V_R vs. θ curves. However, we observe that the only variation in k (where $k > 1$) and ϕ_0 affects the location of these bands. We will now present analytical results to substantiate some of the abovementioned observations.

The following analysis facilitates the identification of these bands. From Eqn. (10), $V_\theta = 0$ yields

$$-\sin\theta - \nu\sin(k\theta + \phi_0) = 0 \tag{12}$$

Hence

$$\theta = \sin^{-1}[-\nu\sin(k\theta + \phi_0)] \tag{13}$$

$\sin^{-1}$ does not exist for $|-\nu\sin(k\theta + \phi_0)| > 1$. Which gives

$$\frac{-1}{\nu} \leq \sin(k\theta_\theta + \phi_0) \leq \frac{1}{\nu} \tag{14}$$

The value of ν will vary for variable speed interceptors, but it must fall within a specific range defined by a minimum value $\nu_{\min}$ and a maximum value $\nu_{\max}$. It is important to identify the maximum possible ν and minimum possible ν for an interceptor to find its capture conditions. To continue this analysis, we will assume that $\nu_{max} = \infty$. Hence, from Eqn. (14), we can write

$$\sin(k\theta_{\theta\infty} + \phi_0) = 0 \tag{15}$$

$$k\theta_{\theta\infty} + \phi_0 = n\pi \tag{16}$$

where $\theta_{\theta\infty}$ represents the roots for V_θ when $\nu = \infty$. Additionally, the variable n takes integer values of 0,±1,±2, and so on, indicating different band numbers. $\theta_{\theta\infty}$ for the n^{th} band is represented by $\theta_{\theta\infty}^{band\, n}$, which is given by

$$\theta_{\theta\infty}^{band\, n} = \frac{n\pi - \phi_0}{k} \tag{17}$$

Similarly, from Eqn. (9)

$$\cos\theta = \nu\cos(k\theta + \phi_0) \tag{18}$$

Eqn. (18) can be used to find $\theta_{R\infty}^{band\, n}$, which represents $\theta_{R\infty}$(the roots for V_R when $\nu = \infty$) for the n^{th} band, which is given by

$$\theta_{R\infty}^{band\, n} = \frac{\frac{(2n-1)\pi}{2} - \phi_0}{k} \tag{19}$$

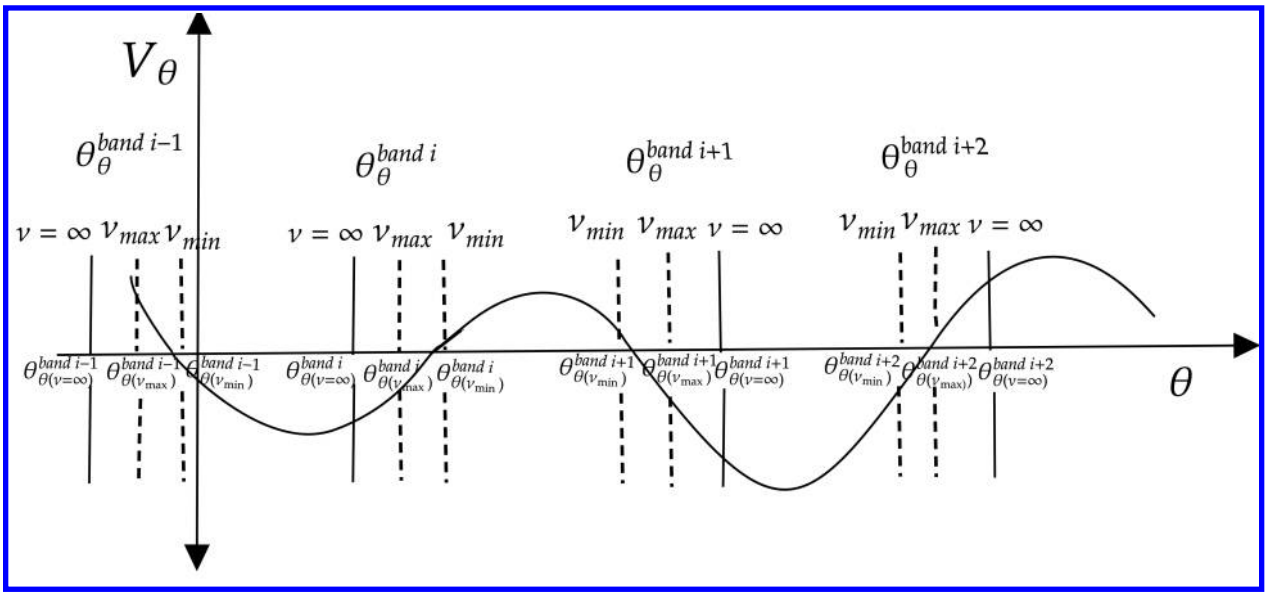

(a)

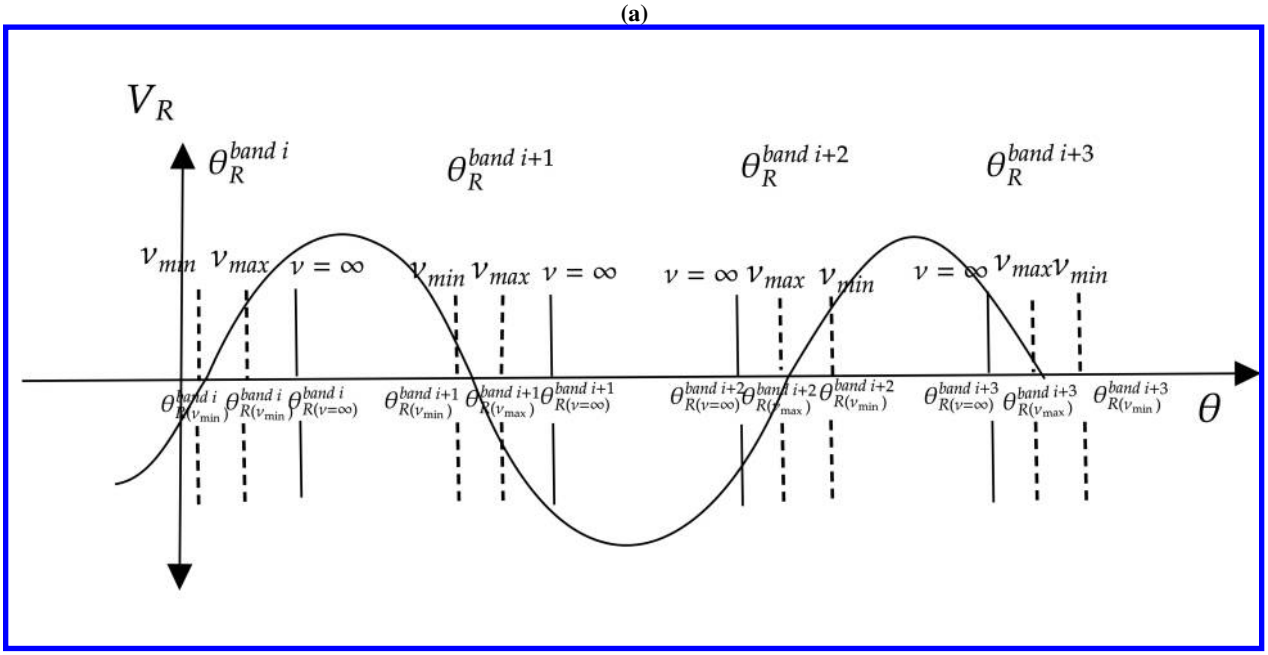

(b)

Fig. 2 Qualitative description: (a) $V_\theta(\theta, \nu)$**, (b)** $V_R(\theta, \nu)$**.**

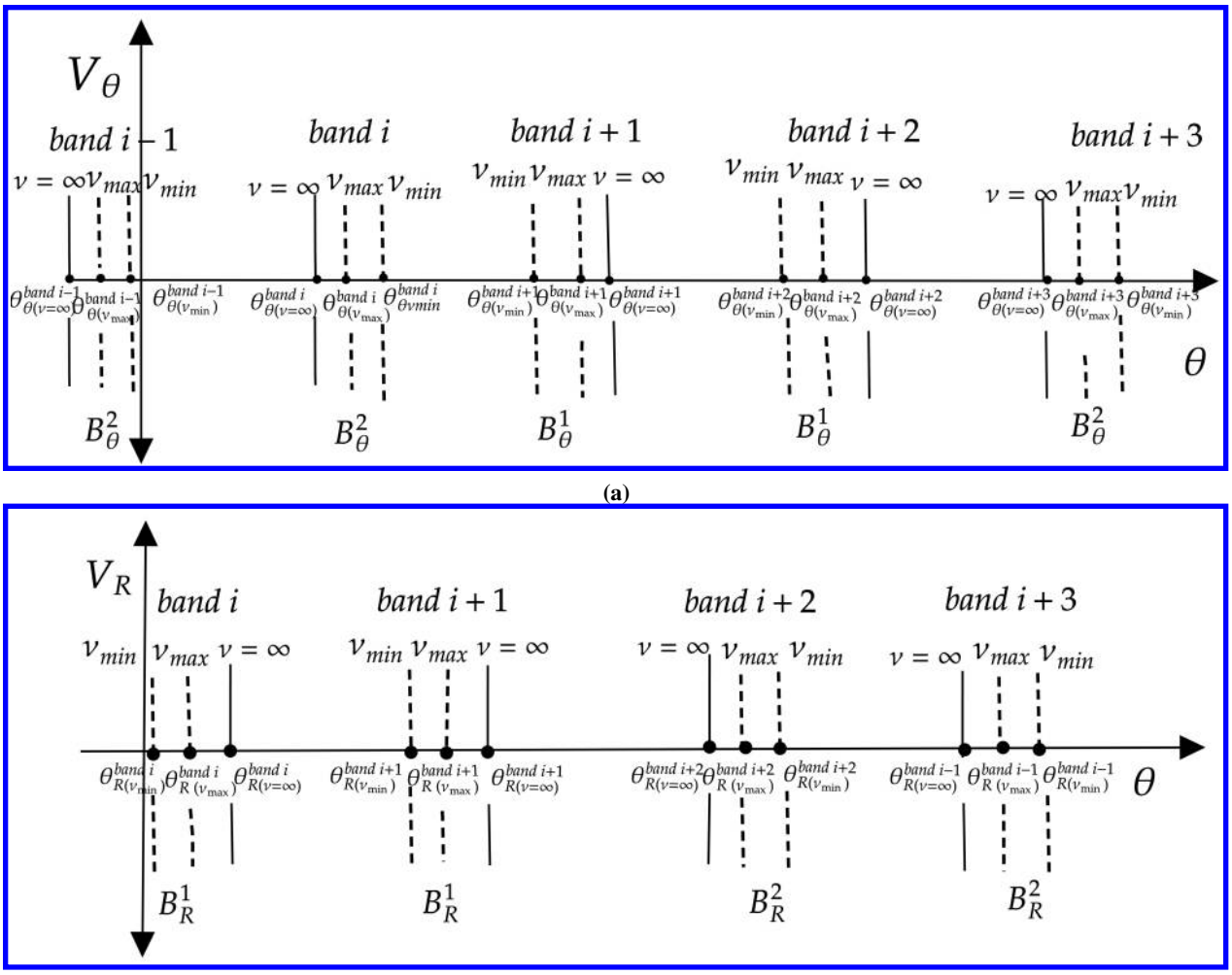

Fig. 3 Band diagram. (a) V_θ **vs.** θ **and , (b)** V_R **vs.** θ

Fig. 3a and Fig. 3b show the band diagrams for V_θ vs. θ and V_R vs. θ, respectively. In Fig. 3a, two categories of bands, B_θ^1 and B_θ^2, are shown. Similarly, in Fig. 3b, two categories of bands B_R^1 and B_R^2 are shown. Those bands are defined as follows.

$$B_\theta^1 = [\theta_\theta(\nu_{\min}), \theta_\theta(\nu_{\max})] \tag{20}$$

In B_θ^1 band θ_θ increases as ν increases from $\nu_{\min}$ to $\nu_{\max}$. If maximum value of $\nu_{\max}$ is extended to ∞ then the band can be defined as

$$B_{\theta\infty}^1 = [\theta_\theta(\nu_{\min}), \theta_\theta(\infty)] \tag{21}$$

Similarly

$$B_\theta^2 = [\theta_\theta(\nu_{\max}), \theta_\theta(\nu_{\min})] \tag{22}$$

In this band θ_θ decreases as ν increases from $\nu_{\min}$ to $\nu_{\max}$. If maximum value of $\nu_{\max}$ is extended to ∞, then the band can be defined as

$$B_{\theta\infty}^2 = [\theta_\theta(\infty), \theta_\theta(\nu_{\min})] \tag{23}$$

Similarly bands for V_R vs. θ curves are defined as follows.

$$B_R^1 = [\theta_R(\nu_{\min}), \theta_R(\nu_{\max})] \tag{24}$$

$$B^1_{R\infty} = [\theta_R(\nu_{\min}), \theta_R(\infty)] \tag{25}$$

In these bands θ_R increases as ν increases from $\nu_{\min}$ to $\nu_{\max}$. Similarly

$$B^2_R = [\theta_R(\nu_{\max}), \theta_R(\nu_{\min})] \tag{26}$$

$$B^2_{R\infty} = [\theta_R(\infty), \theta_R(\nu_{\min})] \tag{27}$$

In these bands θ_R decreases as ν increases from $\nu_{\min}$ to $\nu_{\max}$.
There is a lower bound on ν ($\nu > 1$, given by Lemmas 1 and 2). Substituting this lower bound $\nu = 1$ in Eqn 14, we get

$$\sin^{-1}(-1) \leq (k\theta + \phi_0) + n\pi \leq \sin^{-1}(1) \tag{28}$$

$$2n\pi - \frac{\pi}{2} \leq (k\theta + \phi_0) + n\pi \leq 2n\pi + \frac{\pi}{2} \tag{29}$$

Here, θ represents $\theta_\theta(\nu_{\min} = 1)$. Hence,

$$\frac{n\pi - \frac{\pi}{2} - \phi_0}{k} \leq \theta_\theta(\nu_{\min}) \leq \frac{n\pi + \frac{\pi}{2} - \phi_0}{k} \tag{30}$$

Eqn. (30) represents the possible range for θ_θ for $\nu_{\min}$. Similarly, the range for θ_R for the lower bound on ν ($\nu > 1$, given by Lemma 1 and 2) can be calculated from Eqn. (9) as follows.

$$\frac{-1}{\nu} \leq \cos(k\theta + \phi_0) \leq \frac{1}{\nu} \tag{31}$$

$$\frac{-1}{\nu} \leq \sin\left(\frac{\pi}{2} + k\theta + \phi_0\right) \leq \frac{1}{\nu} \tag{32}$$

At $\nu = 1$

$$\sin^{-1}\left(\frac{-1}{1}\right) \leq n\pi + \frac{\pi}{2} + k\theta + \phi_0 \leq \sin^{-1}\left(\frac{1}{1}\right) \tag{33}$$

$$2n\pi - \frac{\pi}{2} \leq n\pi + \frac{\pi}{2} + k\theta + \phi_0 \leq 2n\pi + \frac{\pi}{2} \tag{34}$$

Here, θ represents $\theta_R(\nu_{\min} = 1)$. Hence

$$\frac{(n-1)\pi - \phi_0}{k} \leq \theta_R(\nu_{min}) \leq \frac{n\pi - \phi_0}{k} \tag{35}$$

Eqn. (35) represents the possible range of θ_R for $\nu_{\min}$.
Lemma 3. If ν lies in $[\nu_{\min}, \nu_{\max}]$, then the roots of V_θ and V_R for the n^{th} band lie $\theta^{band\ n}_\theta = [\theta^{band\ n}_{\theta_{\min}}, \theta^{band\ n}_{\theta_{\max}}]$ and $\theta^{band\ n}_R = [\theta^{band\ n}_{R_{\min}}, \theta^{band\ n}_{R_{\max}}]$ respectively.
Proof. From Eqns. (12) and (18), we will get two different functions for ν

$$\nu_\theta(\theta) = \frac{-\sin\theta}{\sin(k\theta + \phi_0)} \tag{36}$$

$$\nu_R(\theta) = \frac{\cos\theta}{\cos(k\theta + \phi_0)} \tag{37}$$

where, $\nu_\theta(\theta)$ is a function of ν for $V_\theta = 0$ and and it has singular points when $\theta = \frac{n\pi - \phi_0}{k}$. Similarly, $\nu_R(\theta)$ is a function for ν for $V_R = 0$ and it has singularities when $\theta = \frac{\frac{(2n-1)\pi}{2} - \phi_0}{k}$. These functions are continuous for all θ except on the singular points. The Intermediate Value Theorem [42] states that if a function $f(x)$ is continuous on a closed interval $[a, b]$, and if y_0 is any number between $f(a)$ and $f(b)$, then there exists at least one value c in the interval $[a, b]$ such that $f(c) = y_0$. In other words, if a function is continuous on an interval, it takes on all intermediate values between its endpoint values. By the intermediate value theorem, we know that for any value of ν between $\nu_{min} = \frac{-\sin\theta_\theta(\nu_{\min})}{\sin(k\theta_\theta(\nu_{\min})+\phi_0)}$ and $\nu_{max} = \frac{-\sin\theta_\theta(\nu_{\max})}{\sin(k\theta_\theta(\nu_{\max})+\phi_0)}$ there exists a corresponding value of θ_θ between θ_{min} and θ_{max}. This is because the function ν_θ is continuous and takes on all values between ν_{min} and ν_{max} as θ varies between θ_{min} and θ_{max}. Therefore, for any value of ν in the range of the function, the corresponding value of θ_θ lies between θ_{min} and θ_{max}.

Lemma 4. A variable speed interceptor pursuing a non-maneuvering target and following PPN guidance law with $\nu > 1$ and $k\nu > 1$, then the bands B^1_θ, B^2_θ, B^1_R, and B^2_R will not overlap each other.

Proof. There are three possible categories of overlapping.

Case A: Overlapping between bands in V_θ vs. θ.

Case B: Overlapping between bands in V_R vs. θ .

Case C: Overlapping between bands of V_θ vs. θ with bands of V_R vs. θ .

This section discusses all the cases one by one.

Case A: Overlapping between bands in V_θ vs. θ.

Fig. 3a illustrates four combinations of adjacent bands on the V_θ vs. θ curve: two adjacent B^1_θ bands, two adjacent B^2_θ bands, B^1_θ followed by B^2_θ in the same order, and B^2_θ followed by B^1_θ. Eqn. (30) gives the θ_θ corresponds to the lowest ν (here $\nu = 1$). But it has two boundary values, $\frac{n\pi-\frac{\pi}{2}-\phi_0}{k}$ and $\frac{n\pi+\frac{\pi}{2}-\phi_0}{k}$. Selection of boundary value $\theta_\theta(\nu_{\min})$ depends on the category of the band. In B^1_θ band, θ_θ increases as ν increases from $\nu_{\min}$ to ν_∞. Since $\theta_\theta(\nu = \infty)$ is already calculated in Eqn. (17) as $\frac{n\pi-\phi_0}{k}$, $\nu_{\min}$ should be lesser than $\frac{n\pi-\phi_0}{k}$. Hence, possible value for $\nu_{\min}$ in B^1_θ from Eqn. (30) is $\frac{n\pi-\frac{\pi}{2}-\phi_0}{k}$. Similarly ($\frac{n\pi+\frac{\pi}{2}-\phi_0}{k}$) can be used as $\theta_\theta(\nu_{\min})$ for band B^2_θ. These limiting values are also used to discuss the conditions of non-overlapping between two adjacent bands in the V_θ vs. θ curve.

A1. Condition of non-overlap between two adjacent B^1_θ bands.

Two adjacent B^1_θ bands given in Fig. 3a are Band $i+1$ and Band $i+2$. Let us consider $i+1$ is the n^{th} and $i+2$ is $n+1^{th}$ band. The condition for non-overlap between these bands is obtained from Fig. 3a given as

$$\theta^{band\ (n+1)}_{\theta(\nu_{\min})} - \theta^{band\ n}_{\theta(\nu=\infty)} \geq 0 \tag{38}$$

Substituting from Eqns. (17) and (30),

$$\frac{(n+1)\pi - \frac{\pi}{2} - \phi_0}{k} - \frac{n\pi - \phi_0}{k} = \frac{\pi}{2k} \tag{39}$$

Hence, inequality in Eqn (38) is a valid inequality from Eqn. (39) and the gap between two adjacent B^1_θ bands is calculated as $\frac{\pi}{2k}$. Hence two adjacent B^1_θ bands will not overlap.

A2. Condition of non-overlap between two adjacent B^2_θ bands.

Two adjacent B^2_θ bands given in Fig. 3a are Band $i-1$ and Band i. Let us consider $i-1$ is the n^{th} and i is $n+1^{th}$ band. The condition of non-overlap between these bands is obtained from Fig. 3a given as

$$\theta^{band\ (n+1)}_{\theta(\nu=\infty)} - \theta^{band\ n}_{\theta(\nu_{\min})} \geq 0 \tag{40}$$

Substituting from Eqns. (17) and 30,

$$\frac{(n+1)\pi - \phi_0}{k} - \frac{n\pi + \frac{\pi}{2} - \phi_0}{k} = \frac{\pi}{2k} \tag{41}$$

Hence, inequality in Eqn. (40) is a valid inequality from Eqn. (41) and the gap between two adjacent B^2_θ bands is calculated as $\frac{\pi}{2k}$. Hence, two adjacent B^2_θ bands will not overlap.

A3. Condition of non-overlap between B^1_θ followed by B^2_θ.

Two bands which obey the condition B^1_θ followed B^2_θ given in Fig. 3a are Band $i+2$ and Band $i+3$. Let us consider $i+2$ is the n^{th} and $i+3$ is $n+1^{th}$ band. The condition of non-overlap between these bands is obtained from Fig. 3a given as

$$\theta^{band\ (n+1)}_{\theta(\nu=\infty)} - \theta^{band\ n}_{\theta(\nu=\infty)} \geq 0 \tag{42}$$

Substituting from Eqn. (17),

$$\frac{(n+1)\pi - \phi_0}{k} - \frac{n\pi - \phi_0}{k} = \frac{\pi}{k} \tag{43}$$

Hence, inequality in Eqn (42) is a valid inequality from Eqn. (43) and the gap between these bands is calculated as $\frac{\pi}{k}$. Hence, these bands will not overlap.

A4. Condition of non-overlap between B^2_θ followed by B^1_θ.

Two bands which obey the condition B^2_θ followed B^1_θ given in Fig. 3a are Band i and Band $i+1$. Let us consider i is the n^{th} and $i+1$ is $n+1^{th}$ band. The condition of non-overlap between these bands is obtained from Fig. 3a given as

$$\theta^{band\ (n+1)}_{\theta(\nu_{\min})} - \theta^{band\ n}_{\theta(\nu_{\min})} - \geq 0 \tag{44}$$

Substituting from Eqn. (30),

$$\frac{(n+1)\pi - \frac{\pi}{2} - \phi_0}{k} - \frac{n\pi + \frac{\pi}{2} - \phi_0}{k} = 0 \tag{45}$$

Eqn. (45) indicates that the boundaries of bands in this condition may touch each other at $\nu = 1$. But Lemma 1 says $\nu > 1$ and B^1_θ and B^2_θ show opposite variations in θ_θ when ν increases. Hence, these bands will never overlap when $\nu > 1$

Case B. Overlapping between bands V_R vs. θ .

Fig. 3b illustrates four combinations of adjacent bands on the V_R vs. θ curve:

B1: Two adjacent B^1_R bands.

B2: Two adjacent B^2_R bands.

B3: B^1_R followed by B^2_R.

B4: B^2_R followed by B^1_R.

Eqn. (35) gives two boundary values for $\theta_R(\nu_{\min})$, $\frac{(n-1)\pi-\phi_0}{k}$, and $\frac{n\pi-\phi_0}{k}$. Here, $\frac{(n-1)\pi-\phi_0}{k}$ is used as $\theta_R(\nu_{\min})$ for B^1_R because θ_R increases as ν increases from $\nu_{\min}$ to ν_∞. Since $\theta_R(\nu = \infty)$ is already calculated in Eqn. (19) as $\frac{\frac{2n-1}{2}\pi-\phi_0}{k}$, $\nu_{\min}$ should be lesser than $\frac{\frac{2n-1}{2}\pi-\phi_0}{k}$ for B^1_R (See Fig. 3b) Hence, possible value for $\nu_{\min}$ in B^1_R from Eqn. (35) is $\frac{(n-1)\pi-\phi_0}{k}$. Similarly ($\frac{n\pi-\phi_0}{k}$) can be used as $\theta_R(\nu_{\min})$ for band B^2_R.

B1. Condition of non-overlap between two adjacent B^1_R bands.

Two adjacent B^1_R bands given in Fig. 3b are Band i and Band $i+1$. Let us consider i is the n^{th} and $i+1$ is $n+1^{th}$ band. The condition of non-overlap between these bands is obtained from Fig. 3b given as

$$\theta^{band\ (n+1)}_{R(\nu_{\min})} - \theta^{band\ n}_{R(\nu=\infty)} \geq 0 \tag{46}$$

Substituting from Eqns (19) and (35),

$$\frac{((n+1)-1)\pi - \phi_0}{k} - \frac{\frac{(2n-1)}{2}\pi - \phi_0}{k} = \frac{\pi}{2k} \tag{47}$$

Hence, inequality in Eqn (46) is a valid inequality from Eqn. (47) and the gap between two adjacent B^1_R bands is calculated as $\frac{\pi}{2k}$. Hence, two adjacent B^1_R bands will not overlap.

B2. Condition of non-overlap between two adjacent B^2_R bands.

Two adjacent B^2_R bands given in Fig. 3b are Band $i+2$ and Band $i+3$. Let us consider $i+2$ is the n^{th} and $i+3$ is $n+1^{th}$ band. The condition of non-overlap between these bands is obtained from Fig. 3b given as

$$\theta^{band\ (n+1)}_{R(\nu=\infty)} - \theta^{band\ n}_{R(\nu_{\min})} \geq 0 \tag{48}$$

Substituting from Eqns. (19) and (35),

$$\frac{\frac{2(n+1)-1}{2}\pi - \phi_0}{k} - \frac{n\pi - \phi_0}{k} = \frac{\pi}{2k} \tag{49}$$

Hence, inequality in Eqn. (48) is a valid inequality from Eqn. (49) and the gap between two adjacent B^2_R bands is calculated as $\frac{\pi}{2k}$. Hence, two adjacent B^2_R bands will not overlap.

B3. Condition of non-overlap between B^1_R followed by B^2_R.

Two bands which obey the condition B^1_R followed B^2_R given in Fig. 3b are Band $i+1$ and Band $i+2$. Let us consider $i+1$ is the n^{th} and $i+2$ is $n+1^{th}$ band. The condition of non-overlap between these bands is obtained from Fig. 3b given as

$$\theta^{band\ (n+1)}_{R(\nu=\infty)} - \theta^{band\ n}_{R(\nu=\infty)} \geq 0 \tag{50}$$

Substituting from Eqn (19),

$$\frac{\frac{2(n+1)-1}{2}\pi - \phi_0}{k} - \frac{\frac{2n-1}{2}\pi - \phi_0}{k} = \frac{\pi}{k} \tag{51}$$

Hence, inequality in Eqn (50) is a valid inequality from Eqn. (51) and the gap between these bands is calculated as $\frac{\pi}{k}$. Hence, these bands will not overlap.

B4. Condition of non-overlap between B_R^2 followed by B_R^1.
Two bands which obey the condition B_R^2 followed B_R^1 given in Fig. 3b are Band $i+3$ and Band i (Band i will repeat after Band $i+3$). Let us consider $i+3$ is the n^{th} and i is $n+1^{th}$ band. The condition of non-overlap between these bands is obtained from Fig. 3b given as

$$\theta_{R(\nu_{\min})}^{band\ (n+1)} - \theta_{R(\nu_{\min})}^{band\ n} \geq 0 \tag{52}$$

Substituting from Eqn. (35),

$$\frac{((n+1)-1)\pi - \phi_0}{k} - \frac{n\pi - \phi_0}{k} = 0 \tag{53}$$

Eqn. (53) indicates that the boundaries of bands in this condition may touch each other at $\nu = 1$. But Lemma 1 says $\nu > 1$ and B_R^1 and B_R^2 show opposite variations for θ_R when ν increases. Hence, these bands will never intersect when $\nu > 1$

Case C: Overlapping between bands of V_θ vs. θ with bands of V_R vs. θ .
This section discusses all the possible cross overlapping between the bands of V_θ vs. θ with bands of V_R vs. θ. Fig. 3 will give all possible combinations of adjacent bands.
C1. Condition of non-overlap between B_R^1 followed by B_θ^2.
Two bands that obey the condition B_R^1 followed by B_θ^2 given in Fig. 3 are Band i for B_R^1 and B_θ^2. Let us consider i is the n^{th} Band. The condition of non-overlap between these bands is obtained from Fig. 3 given as

$$\theta_{\theta(\nu=\infty)}^{band\ n} - \theta_{R(\nu=\infty)}^{band\ n} \geq 0 \tag{54}$$

Substituting from Eqns (17) and (19),

$$\frac{n\pi - \phi_0}{k} - \frac{\frac{2n-1}{2}\pi - \phi_0}{k} = \frac{\pi}{2k} \tag{55}$$

Hence, inequality in Eqn (54) is a valid inequality from Eqn. (55) and the gap between these bands is calculated as $\frac{\pi}{2k}$. Hence, these bands will not overlap.
C2. Condition of non-overlap between B_θ^1 followed by B_R^2.
Two bands which obey the condition B_θ^1 followed B_R^2 given in Fig. 3 are Band $i+1$ for B_θ^1 and Band $i+2$ for B_R^2 (or Band $i+2$ for for B_θ^1 and Band $i+3$ for B_R^2). Let us consider B_θ^1 is the n^{th} and B_R^2 is $(n+1)^{th}$ band. The condition of non-overlap between these bands is obtained from Fig. 3 given as

$$\theta_{R(\nu=\infty)}^{band\ (n+1)} - \theta_{\theta(\nu=\infty)}^{band\ n} \geq 0 \tag{56}$$

Substituting from Eqns (17) and (19),

$$\frac{\frac{2(n+1)-1}{2}\pi - \phi_0}{k} - \frac{n\pi - \phi_0}{k} = \frac{\pi}{2k} \tag{57}$$

Hence, inequality in Eqn (56) is a valid inequality from Eqn. (57) and the gap between these bands is calculated as $\frac{\pi}{2k}$. Hence, these bands will not overlap.
C3. Condition of non-overlap between B_R^1 followed by B_θ^1.
Two bands which obey the condition B_R^1 followed B_θ^1 is given in Fig. 3 are Band $i+1$ for B_R^1 and Band $i+1$ for B_θ^1. Let us consider B_θ^1 and B_R^1 are n^{th} bands. The condition of non-overlap between these bands is obtained from Fig. 3 given as

$$\theta_{\theta(\nu_{\min})}^{band\ n} - \theta_{R(\nu=\infty)}^{band\ n} \geq 0 \tag{58}$$

Substituting from Eqns (19) and (30),

$$\frac{n\pi - \frac{\pi}{2} - \phi_0}{k} - \frac{\frac{2n-1}{2}\pi - \phi_0}{k} = 0 \tag{59}$$

Eqn. (59) indicates that the boundaries of bands in this condition may touch each other at $\nu = \infty$ for B_θ^1 and $\nu = 1$ for B_R^1. As $\nu > 1$ and $\nu < \infty$ (since ν can be arbitrarily large value) these two bands never intersect.
C4. Condition of non-overlap between B_R^2 followed by B_θ^2.
Two bands which obey the condition B_R^1 followed B_θ^1 given in Fig. 3 are Band $i+3$ for B_R^2 and Band $i+3$ for B_θ^2. Let us consider B_θ^2 and B_R^2 are the n^{th} bands. The condition of non-overlap between these bands is obtained from Fig. 3 and is given as

$$\theta_{\theta(\nu=\infty)}^{band\ n} - \theta_{R(\nu_{\min})}^{band\ n} \geq 0 \tag{60}$$

Substituting from Eqns (17) and (35),

$$\frac{n\pi - \phi_0}{k} - \frac{n\pi - \phi_0}{k} = 0 \tag{61}$$

Eqn. (61) indicates that the boundaries of bands in this condition may touch each other at $\nu = \infty$ for B^2_θ and $\nu = 1$ for B^2_R. In practice, if $\nu > 1$ and $\nu < \infty$ these two bands never intersect.

C5 and C6. Conditions of non-overlap between B^2_θ followed by B^1_R and B^2_R followed by B^1_θ.

Two bands which obey the condition B^2_θ followed B^1_R is given in Fig. 3. Band $i+1$ for B^1_R and Band i for B^2_θ (and Band i for B^1_R and Band $i-1$ for B^2_θ). Two bands which obey the condition B^2_R followed B^1_θ is given in Fig. 3 are Band $i+2$ for B^2_R and Band $i+2$ for B^1_θ. The conditions are given as

$$\theta^{band\,(n+1)}_{R\nu min} - \theta^{band\,n}_{\theta\nu min} \geq 0 \tag{62}$$

$$\theta^{band\,n}_{\theta\nu min} - \theta^{band\,(n+1)}_{R\nu min} \geq 0 \tag{63}$$

These two conditions are proved using a different approach. If there is an overlap between B^2_θ and B^1_R (or B^2_R and B^1_θ), there will be a ν at which θ_θ=θ_R. This ν can be found out by equating Eqns. (36) and (37)

$$\frac{\cos\theta}{\cos(k\theta + \phi_0)} = \frac{-\sin\theta}{\sin(k\theta + \phi_0)} \tag{64}$$

$$\cos\theta\sin(k\theta + \phi_0) + \sin\theta\cos(k\theta + \phi_0) = 0 \tag{65}$$

$$\sin((k+1)\theta + \phi_0) = 0 \tag{66}$$

$$(k+1)\theta + \phi_0 = n\pi \tag{67}$$

$$k\theta + \phi_0 = n\pi - \theta \tag{68}$$

Substituting Eqn. (68) in Eqns. (36) and (37)

$$\nu_R = \frac{\cos\theta}{\cos(n\pi - \theta)} = \frac{\cos\theta}{\cos n\pi\cos\theta} = \frac{1}{\cos n\pi} = \pm 1 \tag{69}$$

$$\nu_\theta = \frac{-\sin\theta}{\sin(n\pi - \theta)} = \frac{\sin\theta}{\cos n\pi\sin\theta} = \frac{1}{\cos n\pi} = \pm 1 \tag{70}$$

Eqns. 69 and 70 prove that $\theta_\theta = \theta_R$ at $\nu = 1$ (-1 is neglected because speed ratio is always positive). But Lemma 1 say $\nu > 1$ and when ν increases from ν_{min} to ν_{max}, θ_θ and θ_R move in opposite directions (one will increase and the other will decrease) from an angle $\theta_\theta = \theta_R$ at $\nu = 1$. For example, consider the condition B^2_θ followed by B^1_R, which is the adjacency between and Band i for B^1_R in V_R *vs* θ and Band $i-1$ for B^2_θ V_θ *vs* θ. Since band $i-1$ of B^2_θ which shows a property of decreasing θ_θ when ν increases and opposite behaviour for B^1_R in V_R *vs* θ. So we can say that when ν increases from ν_{min} to ν_{max}, θ_θ and θ_R move in opposite directions from a point at which $\nu = 1$. Consequently, the occurrence of any overlap is prevented, ensuring the fulfillment of inequality (62). Similar explanation can be also given for inequality (63). Hence all the conditions of non-overlap are proved.

Lemma 1 shows the roots of V_θ and V_R alternate along the θ axis for a constant ν. But for variable speed interceptor, we need to consider the entire band of θ where the roots of V_θ and V_R lie for different ν.

Lemma 5. Let $\theta^{band\,n}_\theta$ and $\theta^{band\,n}_R$ be the bands of roots of the $V_\theta(\theta,\nu)$ and $V_R(\theta,\nu)$ curves for $\nu\epsilon[\nu_{\min},\nu_{\max}]$, along the θ axis, where $n = 0, \pm1, \pm2, \pm3...$, represents the band numbers. If $\nu > 1$ and $k\nu > 1$ for all $\nu\epsilon[\nu_{\min},\nu_{\max}]$, then the bands of roots of $V_\theta(\theta,\nu)$ and $V_R(\theta,\nu)$ alternate along the θ axis .

Proof Consider Fig. 4, $\theta^{band\,1}_\theta$,$\theta^{band\,2}_\theta$, $\theta^{band\,3}_\theta$... are the bands of roots of V_θ and $\theta^{band\,1}_R$, $\theta^{band\,2}_R$, $\theta^{band\,3}_R$... are the bands of roots of V_R. Lemma 4 explores the characteristics of the bands and shows that there is no overlap between any of them. According to Condition A3 (See Eqn. (43)), the gap between two θ_θ bands is $\frac{\pi}{k}$. Similarly, Condition B3 (See (Eqn. 51)) states that the gap between two θ_R bands is also $\frac{\pi}{k}$. However, the separation between θ_θ and θ_R bands, as indicated by Condition C1 (See Eqn. (55)), is $\frac{\pi}{2k}$. These properties remain valid only if the bands of θ_θ and θ_R alternate in sequence.

Lemma 6. Let $\theta^{band\,n}_\theta$ and $\theta^{band\,n}_R$ be the bands of roots of the $V_\theta(\theta,\nu)$ and $V_R(\theta,\nu)$ curves for $\nu\epsilon[\nu_{\min},\nu_{\max}]$, along the θ axis, If $\nu > 1$ and $k\nu > 1$ for all $\nu\epsilon[\nu_{\min},\nu_{\max}]$, then all the roots θ_θ in that band satisfy the condition

$$V_R(\theta_{\theta 1})\frac{dV_\theta}{d\theta}(\theta_{\theta 1}) > 0 \tag{71}$$

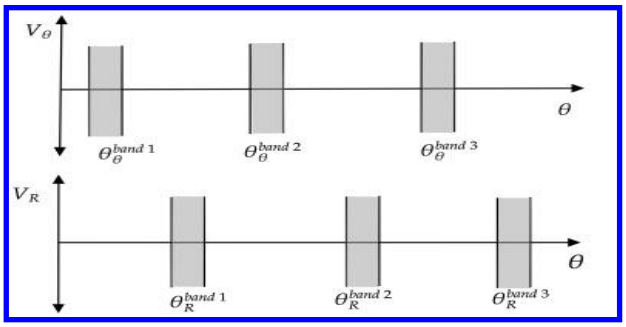

Fig. 4 Band Diagram

Here, $\theta_{\theta 1}$ represents any root within the θ_θ band for $\nu = \nu_1$ where $\nu_1 \epsilon [\nu_{\min}, \nu_{\max}]$.
Proof This lemma can be proved by considering V_θ for ν_1 and V_R for ν_2 where $\nu_2 \epsilon [\nu_{\min}, \nu_{\max}]$.

$$V_\theta(\theta_{\theta 1}) = -\sin\theta_{\theta 1} - \nu_1 \sin(k\theta_{\theta 1} + \phi_0) \tag{72}$$

$$V_R(\theta_{\theta 1}) = \cos\theta_{\theta 1} - \nu_2 \cos(k\theta_{\theta 1} + \phi_0) \tag{73}$$

Differentiating Eqn. (72)

$$\frac{dV_\theta(\theta_{\theta 1})}{d\theta} = -\cos\theta_{\theta 1} - k\nu_1 \cos(k\theta_{\theta 1} + \phi_0) \tag{74}$$

Hence,

$$V_R(\theta_{\theta 1})\frac{dV_\theta(\theta_{\theta 1})}{d\theta} = k\nu_1\nu_2 \cos^2(k\theta_{\theta 1} + \phi_0) - k\nu_1 \cos\theta_{\theta 1}\cos(k\theta_{\theta 1} + \phi_0) + \nu_2 \cos\theta_{\theta 1}\cos(k\theta_{\theta 1} + \phi_0) - \cos^2\theta_{\theta 1} \tag{75}$$

Equating Eqn. (72) to zero, we can formulate

$$k\nu_1\nu_2 \cos^2(k\theta_{\theta 1} + \phi_0) = k\nu_1\nu_2 + k\nu_2 \sin\theta_{\theta 1}\sin(k\theta_{\theta 1} + \phi_0) \tag{76}$$

and

$$\cos^2(\theta_{\theta 1}) = 1 + \nu_1 \sin\theta_{\theta 1}\sin(k\theta_{\theta 1} + \phi_0) \tag{77}$$

Substituting Eqns. (76) and (77) in Eqn. (75)

$$V_R(\theta_{\theta 1})\frac{dV_\theta(\theta_{\theta 1})}{d\theta} = k\nu_1\nu_2 + k\nu_2 \sin\theta_{\theta 1}\sin(k\theta_{\theta 1} + \phi_0) - k\nu_1 \cos\theta_{\theta 1}\cos(k\theta_{\theta 1} + \phi_0) + \nu_2 \cos\theta_{\theta 1}\cos(k\theta_{\theta 1} + \phi_0) - 1 - \nu_1 \sin(\theta_{\theta 1})\sin(k\theta_{\theta 1} + \phi_0) \tag{78}$$

$$V_R(\theta_{\theta 1})\frac{dV_\theta(\theta_{\theta 1})}{d\theta} = k\nu_1\nu_2 - 1 + \sin(k\theta_{\theta 1} + \phi_0)\sin\theta_{\theta 1}(k\nu_2 - \nu_1) - \cos(k\theta_{\theta 1} + \phi_0)\cos\theta_{\theta 1}(k\nu_1 - \nu_2) \tag{79}$$

$$V_R(\theta_{\theta 1})\frac{dV_\theta(\theta_{\theta 1})}{d\theta} = k\nu_1\nu_2 - 1 + \frac{(k\nu_2 - \nu_1)}{2}(\cos((k+1)\theta_{\theta 1} + \phi_0) - \cos((k-1)\theta_{\theta 1} + \phi_0) - \frac{(k\nu_1 - \nu_2)}{2}(\cos((k+1)\theta_{\theta 1} + \phi_0) + \cos((k-1)\theta_{\theta 1} + \phi_0) \tag{80}$$

$$V_R(\theta_\theta)\frac{dV_\theta(\theta_\theta)}{d\theta} = k\nu_1\nu_2 - 1 - (k+1)\frac{\nu_1 - \nu_2}{2}\cos((k+1)\theta_{\theta 1} + \phi_0) - (k-1)\frac{\nu_+\nu_2}{2}\cos((k-1)\theta_{\theta 1} + \phi_0) \tag{81}$$

The satisfaction of $V_R(\theta_\theta)\frac{dV_\theta(\theta_\theta)}{d\theta} > 0$ of Eqn. (81) depends on the values of $\cos((k+1)\theta_{\theta 1}+\phi_0)$ and $\cos((k-1)\theta_{\theta 1}+\phi_0)$. This leads to the existence of four possible conditions, which are described below.
Case 1. $\cos((k+1)\theta_{\theta 1} + \phi_0) = 1$ and $\cos((k-1)\theta_{\theta 1} + \phi_0) = 1$
Hence,

$$(k\nu_1\nu_2 - 1) - (k+1)\frac{\nu_1 - \nu_2}{2} - (k-1)\frac{\nu_1 + \nu_2}{2} > 0 \tag{82}$$

$$(\nu_2 - 1)(k\nu_1 + 1) > 0 \tag{83}$$

which is satisfied when $\nu_2 > 1$
Case 2. $\cos((k+1)\theta_{\theta 1} + \phi_0) = 1$ and $\cos((k-1)\theta_{\theta 1} + \phi_0) = -1$
Hence,

$$(k\nu_1\nu_2 - 1) - (k+1)\frac{\nu_1 - \nu_2}{2} + (k-1)\frac{\nu_1 + \nu_2}{2} > 0 \tag{84}$$

$$(\nu_1 + 1)(k\nu_2 - 1) > 0 \tag{85}$$

which is satisfied when $k\nu_2 > 1$
Case 3. $\cos((k+1)\theta_{\theta 1} + \phi_0) = -1$ and $\cos((k-1)\theta_{\theta 1} + \phi_0) = 1$
Hence,

$$(k\nu_1\nu_2 - 1) + (k+1)\frac{\nu_1 - \nu_2}{2} - (k-1)\frac{\nu_1 + \nu_2}{2} > 0 \tag{86}$$

$$(\nu_1 - 1)(k\nu_2 - 1) > 0 \tag{87}$$

which is satisfied when $\nu_1 > 1$ and $k\nu_2 > 1$.
Case 4. $\cos((k+1)\theta_{\theta 1} + \phi_0) = -1$ and $\cos((k-1)\theta_{\theta 1} + \phi_0) = -1$
Hence,

$$(k\nu_1\nu_2 - 1) + (k+1)\frac{\nu_1 - \nu_2}{2} + (k-1)\frac{\nu_1 + \nu_2}{2} > 0 \tag{88}$$

$$(\nu_2 + 1)(k\nu_1 - 1) > 0 \tag{89}$$

which is satisfied when $k\nu_1 > 1$
In summary, if $\nu_1 > 1$,$\nu_2 > 1$, $k\nu_1 > 1$, and $k\nu_2 > 1$, then $V_R(\theta_{\theta 1})\frac{dV_\theta(\theta_{\theta 1})}{d\theta} > 0$

IV. Capture Conditions

This section will determine the conditions under which the interceptor can successfully intercept the target. This analysis considers a varying speed interceptor that employs the PPN guidance law in an attempt to capture a non-maneuvering target. Consider the Fig. 5, It is possible to identify the following bands. which do not overlap, as shown in the analysis in the previous section.

$$\begin{aligned}
B_\theta^{1+} &= \{\theta : \theta \epsilon B_\theta^1, V_R(\theta, \nu) > 0\} \\
B_\theta^{1-} &= \{\theta : \theta \epsilon B_\theta^1, V_R(\theta, \nu) < 0\} \\
B_\theta^{2+} &= \{\theta : \theta \epsilon B_\theta^2, V_R(\theta, \nu) > 0\} \\
B_\theta^{2-} &= \{\theta : \theta \epsilon B_\theta^2, V_R(\theta, \nu) < 0\} \\
B_R^{1+} &= \{\theta : \theta \epsilon B_R^1, V_\theta(\theta, \nu) > 0\} \\
B_R^{1-} &= \{\theta : \theta \epsilon B_R^1, V_\theta(\theta, \nu) < 0\} \\
B_R^{2+} &= \{\theta : \theta \epsilon B_R^2, V_\theta(\theta, \nu) > 0\} \\
B_R^{2-} &= \{\theta : \theta \epsilon B_R^2, V_\theta(\theta, \nu) < 0\}
\end{aligned} \tag{90}$$

$$\begin{aligned}
\sigma_{\theta\,\min}^{+} &= \{\theta : V_\theta(\theta, \nu) > 0, \nu = \nu_{\min}\} \\
\sigma_{\theta\,\max}^{+} &= \{\theta : V_\theta(\theta, \nu) > 0, \nu = \nu_{\max}\} \\
\sigma_{\theta\,\min}^{-} &= \{\theta : V_\theta(\theta, \nu) < 0, \nu = \nu_{\min}\} \\
\sigma_{\theta\,\max}^{-} &= \{\theta : V_\theta(\theta, \nu) < 0, \nu = \nu_{\max}\} \\
\sigma_{R\,\min}^{+} &= \{\theta : V_R(\theta, \nu) > 0, \nu = \nu_{\min}\} \\
\sigma_{R\,\max}^{+} &= \{\theta : V_R(\theta, \nu) > 0, \nu = \nu_{\max}\} \\
\sigma_{R\,\min}^{-} &= \{\theta : V_R(\theta, \nu) < 0, \nu = \nu_{\min}\} \\
\sigma_{R\,\max}^{-} &= \{\theta : V_R(\theta, \nu) < 0, \nu = \nu_{\max}\}
\end{aligned} \tag{91}$$

The conditions for interception are well-defined in the literature. If $V_\theta = 0$ and $V_R < 0$, the interceptor is on a collision course. Conversely, if $V_\theta = 0$ and $V_R > 0$, the interceptor is on an inverse collision course. In our analysis, B_θ^{1-}

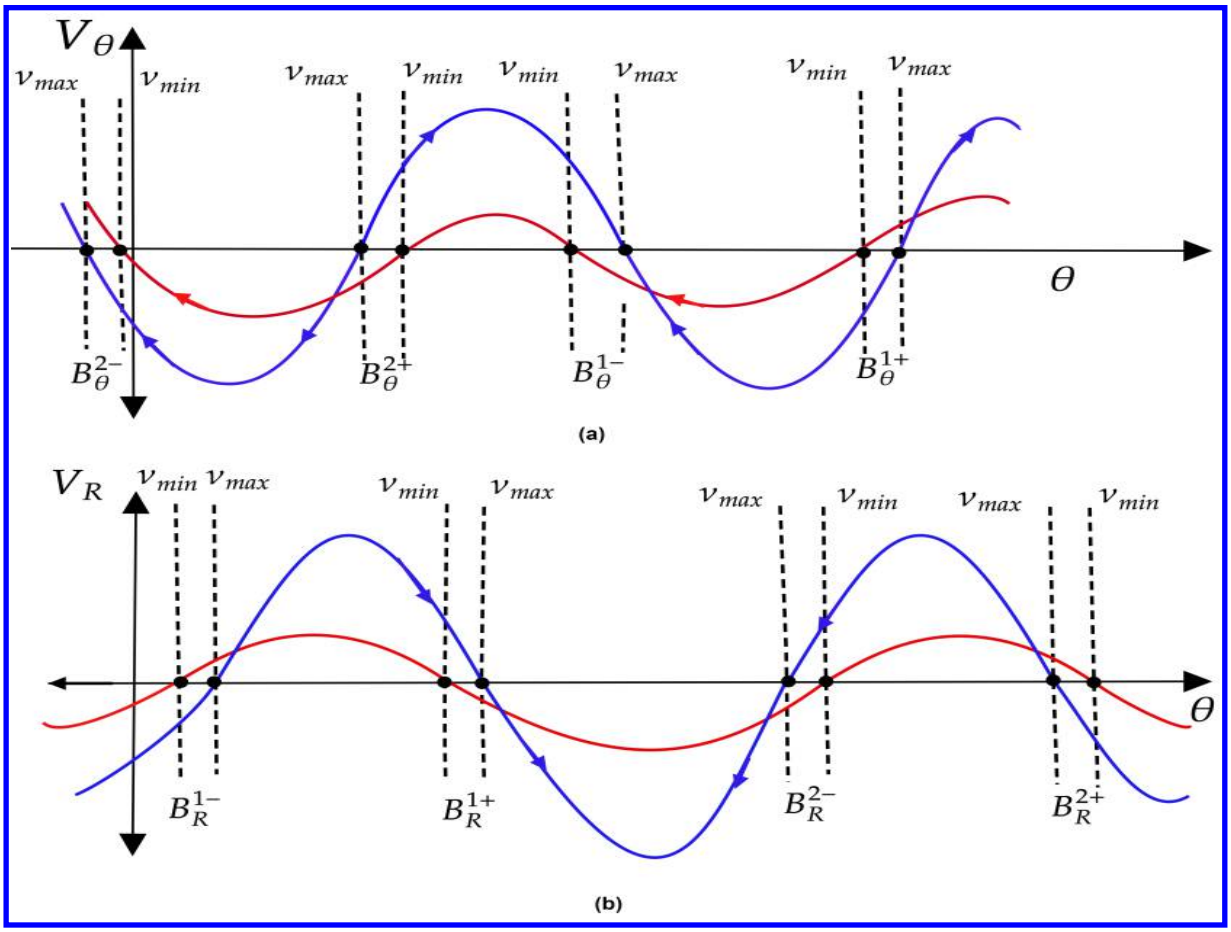

Fig. 5 Band Diagram. (a) V_θ **vs.** θ **and , (b)** V_R **vs.** θ

and B_θ^{2-} are the bands where the roots θ_θ inside these bands are stable fixed points (equilibrium points). The roots in B_θ^{1-} and B_θ^{2-} for a given $\nu \in [\nu_{\min}, \nu_{\max}]$ represent the collision course because roots in these regions have $V_\theta = 0$ and $V_R < 0$ (see Fig. 5). However, since ν can vary between the given limits as the interceptor approaches the target, the actual root at which the interception occurs may vary within the band. The fact that inside the band $V_R < 0$, irrespective of what the value of ν is, ensures that interception will eventually happen. It is clear from the graphs given in Fig. 5 that, whatever the initial point outside the B_θ^{1+} and B_θ^{2+} bands, they move to the collision course in the direction of the arrows provided in the graph. Similarly, the roots in B_θ^{1+} and B_θ^{2+} have unstable equilbrium points. The roots in B_θ^{1+} and B_θ^{2+} represent the case when $V_R > 0$ with the possibility of V_θ becoming zero thus leading to inverse collision course. Although there is a possibility that the point may come out of these bands, but still interception cannot be guaranteed inside these bands. (see Fig. 5).

Before we state the main theorem of the paper, we need to consider a few special cases. Velocity of the interceptor may vary either gradually or through sudden changes, such as switching between two velocities. The most extreme circumstance for the investigation of the variable speed interceptor is switching between two extreme velocities. In this paper, we investigate switching between maximum and minimum velocities of the interceptor, which will account for the challenges posed by gradual changes in speed and velocity switching inside the minimum-maximum limits.

We can identify several types of velocity switching for the interceptor from the Fig. 6 given as follows.

1) *Switching the velocity ratio from* $\nu_{\max}$ *to* $\nu_{\min}$ *outside the* B_θ^{1-} *and* B_θ^{2-} *bands:* It is represented by switching from a to a' in the Figure 6. Even though it changes the curve for $\nu_{\max}$ to $\nu_{\min}$ the behaviour of both the graphs remains the same for a and a'. When switching happens from $\nu_{\max}$ to $\nu_{\min}$ graph shifts from a to a' and continues towards the collision course point at o_1 instead of o. The same scenario is also depicted in the polar plane, as shown in Figure 7. It illustrates the identical behavior as described earlier. In practical terms, when the switching happens from $\nu_{\max}$ to $\nu_{\min}$, the speed of the interceptor obviously reduces, and as a result, the rate of reduction of

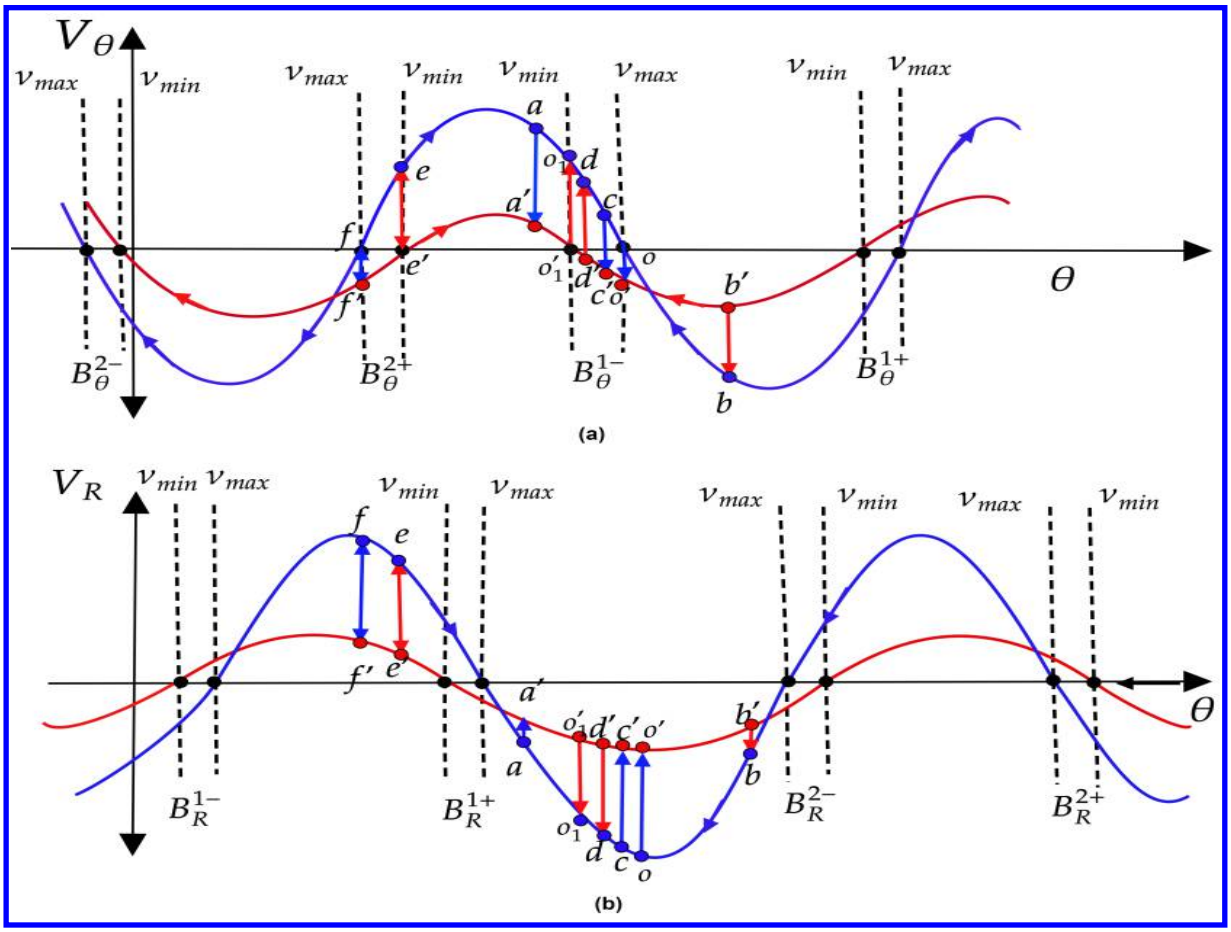

Fig. 6 Switching Diagram. (a) V_θ **vs.** θ **and , (b)** V_R **vs.** θ

R and θ also reduces. However, it will still reach the collision course at o_1.

2) *Switching the velocity ratio from* $\nu_{\min}$ *to* $\nu_{\max}$ *outside the* B_θ^{1-} *and* B_θ^{2-} *bands:* This situation is demonstrated in Figure 6 by the switching from b' to b. Both graphs show a similar trend, that is, they move towards B_θ^{1-} band and the paths are shown in Figure 6 by an arrow. Finally, it reaches the stable point o instead of o_1. From a practical point of view, when the velocity of the interceptor increases, magnitude V_θ and V_R also increase which may result in faster interception.
3) *Switching the velocity ratio from* $\nu_{\max}$ *to* $\nu_{\min}$ *inside the* B_θ^{1-} *and* B_θ^{2-} *bands:* The scenario depicted in Figure 6 shows the switching from c to c'. where V_θ crosses the θ axis and changes its positive value to a negative value but it does not become zero. The interceptor then follows the path of $\nu_{\min}$ and eventually reaches the collision course at o_1. In a practical sense, when the interceptor changes its speed within the stable bands it needs to apply lateral acceleration opposite to the prior lateral acceleration direction to change the direction of V_θ.
4) *Switching the velocity ratio from* $\nu_{\min}$ *to* $\nu_{\max}$ *inside the* B_θ^{1-} *and* B_θ^{2-} *bands:* This situation is illustrated in Figure 6 by the switching from d to d'. When the switch occurs, V_θ crosses the θ axis and changes from a negative value to a positive value but it does not become zero. The interceptor then follows the path of $\nu_{\max}$ and ultimately reaches the collision course at o. This behaviour is also presented in the polar plane (see Figure 7). In a practical sense, when the interceptor changes its speed within the stable bands, it needs to apply a lateral acceleration in the opposite direction to the prior lateral acceleration in order to change the direction of V_θ.
5) *Switching the velocity ratio from* $\nu_{\max}$ *to* $\nu_{\min}$ *at the root* $\theta_\theta(\nu_{\max})$ *and switching the velocity ratio from* $\nu_{\min}$ *to* $\nu_{\max}$ *at the root* $\theta_\theta(\nu_{\min})$*:* The switching point o is used for switching from $\nu_{\max}$ to $\nu_{\min}$ and o_1 i is used for switching from $\nu_{\min}$ to $\nu_{\max}$ as shown in Figure 6. The point o and o_1 are considered as the roots of the graphs for $\nu_{\max}$ and $\nu_{\min}$, respectively, which are stable nodes indicating that the collision course starts at those conditions. Any disturbance on V_θ will not affect the collision course because the interceptor is at a stable root and it will

return to the collision course at the same root. However, changing ν causes a change in the equilibrium point. When ν switches from $\nu_{\max}$ to $\nu_{\min}$, the graph jumps from o to o' and follows the path of $\nu_{\min}$, so that, finally the collision course starts at o_1. If the switching happens from o_1' to o_1 it will follow the path of $\nu_{\max}$, so that, finally the collision course starts at o. The physical interpretation is that, a change in the interceptor velocity disturbs the collision course, and then, its V_θ changes so as to achieve a new collision course with a new interception angle.

6) *Switching the velocity ratio from $\nu_{\max}$ to $\nu_{\min}$ and $\nu_{\min}$ to $\nu_{\max}$ at corresponding roots in the unstable bands B_θ^{2+} andB_θ^{1+}:* The roots inside the bands B_θ^{2+} and B_θ^{1+} correspond to inverse collision course. Consider the point e' which corresponds to the unstable root for $\nu_{\min}$ when ν switches to $\nu_{\max}$ it moves away from the inverse collision course and eventually reaches the collision course at point o. Similarly, when switching occurs at f from $\nu_{\max}$ to $\nu_{\min}$ which is the unstable root for $\nu_{\max}$ it moves away from inverse collision course and reaches the collision course point in the B_θ^{2-} band. Hence, it can be concluded that even small changes in velocity can alter the inverse collision course, even if the roots are within the B_θ^{2+} and B_θ^{1+} bands. As a result of the velocity change, the collision course may be attained at a different band.
7) *Switching the velocity ratio from $\nu_{\max}$ to $\nu_{\min}$ and $\nu_{\min}$ to $\nu_{\max}$ to reach inverse collision course:* Consider an engagement with a velocity ratio $\nu_{\max}$ which reaches the point e in Figure 6. If we switch to $\nu_{\min}$, the reaching point becomes an inverse collision course. Similarly, if we move along the path of $\nu_{\min}$ which reaches at f' and if we switch to $\nu_{\max}$ it will reach f, which is also an inverse collision course. Inference is that when the interceptor is in B_θ^{2+} and B_θ^{1+} bands, the velocity changes may cause the interceptor to go to an inverse collision course.
8) *Finite number of switching inside the stable bands:* If we consider a finite number of switches within the B_θ^{1-} and B_θ^{2-} bands, it is observed that the interceptor crosses the θ axis a finite number of times. It will never reach the collision triangle until the switching stops. For instance, when the interceptor switches at c, it moves to c' and continues the path of $\nu_{\min}$ bands in the direction of the arrow. When it reaches the switching point d', if we allow it to switch to d, it will reach d and follow the path of V_{max} and loops the path c, c', d', d, if we follow a similar switching pattern. The last switching will determine the path towards the collision triangle. If it reaches c', it will follow the path of the $\nu_{\min}$ and if it reaches d, it will follow the path of the $\nu_{\min}$, as shown in Figure 6.
9) *Infinite number of switching inside the stable bands:* This case is complex, and we do not have results for it, although it might be possible to prove convergence to collision under certain circumstances. But we point out that it is an unrealistic case in a real scenario.

Theorem 1. A variable speed interceptor pursuing a non-maneuvering target and following PPN guidance law with $\nu > 1$ and $k\nu > 1$ will be able to capture the target from all initial conditions lying outside the B_θ^{1+} and B_θ^{2+} bands, with the possible exception of infinite number of speed ratio switching inside the bands B_θ^{1-} and B_θ^{2-} during the engagement.

Proof. Lemma 5 and Lemma 6 will give sufficient conditions to prove Theorem 2. Fig. 6 and 7 can be used to arrive at a result that all the initial conditions except for the bands B_θ^{1+} and B_θ^{2+} will move to the collision bands in B_θ^{1-} and B_θ^{2-} independent of any speed variations except infinite switching of speed ratio between the two minimum and maximum values inside B_θ^{1-} and B_θ^{2-}. Lemma 5 and Lemma 6 ensure that any change in ν will not cause change in the value of V_R from $V_R < 0$ to $V_R > 0$ because all the changes in ν inside the B_θ^{1-} and B_θ^{2-} happens with the condition that $V_R < 0$. The switching Cases from 1-5 and 8 also prove Theorem 1. Case 9 describes the switching of speed ratio inside the capture bands (B_θ^{1-} and B_θ^{2-}).

Theorem 2. If the initial position of the interceptor is inside the B_θ^{1+} and B_θ^{2+} bands, It leaves these bands. It intercepts the target when the velocity changes, except for the velocity changes towards the inverse collision course.

Proof. The bands B_θ^{1+} and B_θ^{2+} exhibit a property where both σ_{Rmax} and σ_{Rmin} are greater than zero. As a result, the interceptor follows an inverse collision course when located within these bands. However, a change in velocity causes the interceptor to deviate from the inverse collision course and enter the (B_θ^{1-} and B_θ^{2-}) bands. This engagement scenario is illustrated in Fig. 6 and Fig. 7, specifically in the switching case described in Case 6, transitioning from e' to e and ultimately reaching o. It is important to note that if any switching occurs similar to Case 7 (e to e' or f' to f), the interceptor will resume an inverse collision course.

Corollary 1. An inverse collision course can be achieved only B_θ^{1+} and B_θ^{2+}.

Proof. Any variation outside the band will not allow the interceptor to re-enter into B_θ^{1+} and B_θ^{2+} bands (see Fig. 6) hence it is possible to say that the inverse collision course will be achieved only in these bands.

Corollary 2. Once the interceptor enters the B_θ^{1-} and B_θ^{2-} bands, it is impossible to maneuver the interceptor outside of these bands through velocity variations.

Proof. Fig. 6 and 7 give an insight that whatever the velocity changes inside the (B_θ^{1-} and B_θ^{2-}) causes the interceptor jump from one point to another inside the corresponding band only. Hence, it is possible to claim that interception is guaranteed inside the (B_θ^{1-} and B_θ^{2-}) bands except perhaps for the infinite switching case.

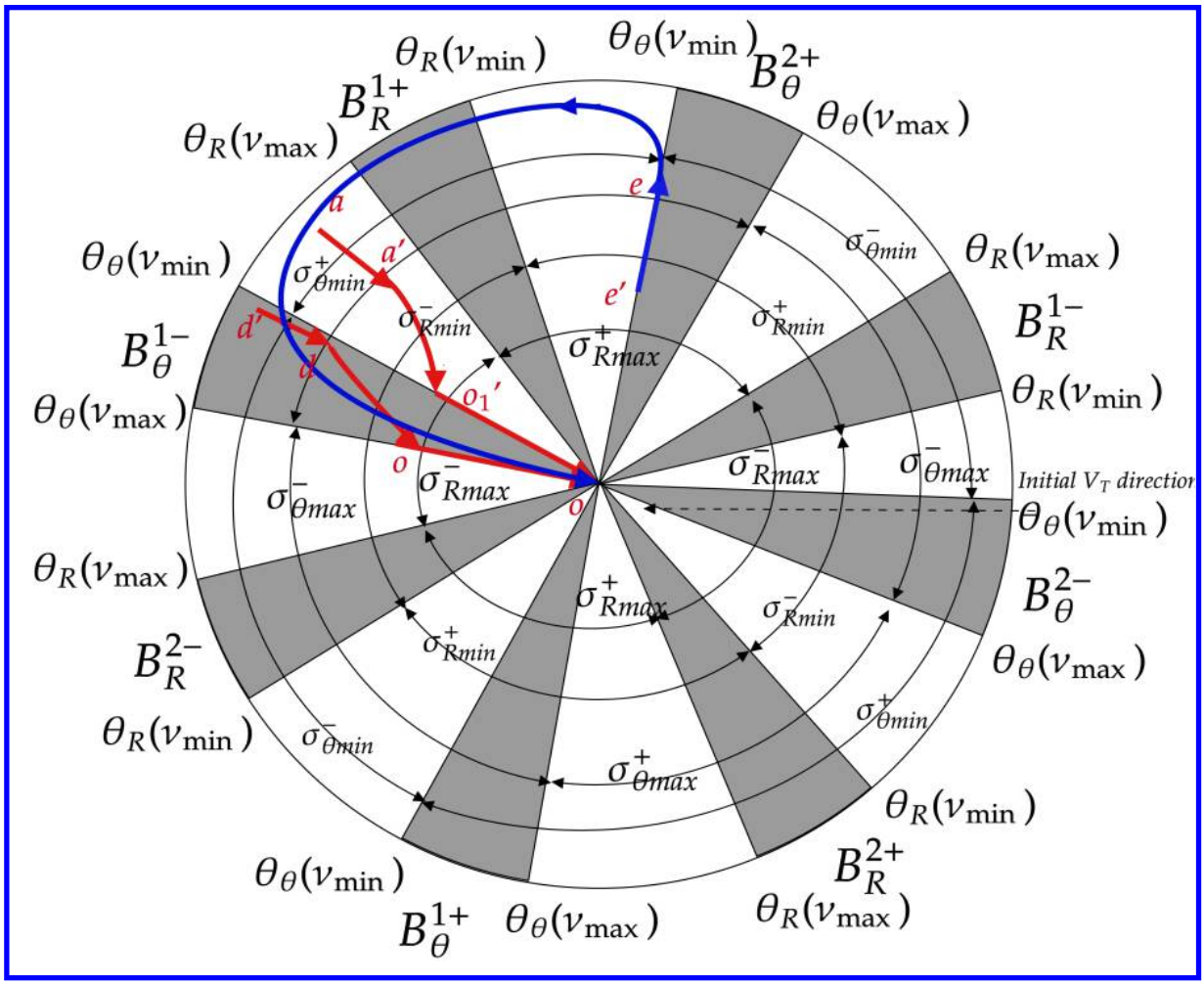

Fig. 7 A representation of the roots $V_R(\theta, \nu)$ and $V_\theta(\theta, \nu)$ in polar plane.

Corollary 3. It is possible to control the interception angle between $\theta_\theta(\nu_{\min})$ and $\theta_\theta(\nu_{\max})$ by varying the speed of the interceptor.

Proof. Based on the observations depicted in Figure 6 and 7, it is evident that once the interceptor reaches the collision course, it gradually converges towards the target along the θ_θ line. Furthermore, any variations in velocity lead to corresponding changes in the θ_θ value, which ranges between $\theta_\theta(\nu_{\min})$ and $\theta_\theta(\nu_{\max})$.

V. Conclusions

This paper gives a qualitative analysis of a variable speed PPN guidance law against a non-maneuvering target. The bands of the line of sight angle, in which the relative components of velocity become zero, are defined, and the properties of these bands are described. These properties define capture conditions for a variable speed PPN guidance law against a non-maneuvering target. The method for capturing a non-maneuvering target, even if the interceptor target engagement is on an inverse collision course, is also discussed. We employed velocity switching between the maximum and minimum velocities of the interceptor, encompassing the complexities arising from gradual changes in speed and velocity transitions within the prescribed limits. Future work will involve extending the qualitative analysis of the variable speed PPN guidance law against maneuvering targets and targets that have both maneuvering and non-maneuvering phases in their engagement. Additionally, determining the capture conditions with a variable speed PPN guidance law when the interceptor's speed is lower than the target is also an interesting future direction of research.

References

[1] Zarchan, P., *Tactical and Strategic Missile Guidance*, Vol. 239, American Institute of Aeronautics and Astronautics, Inc., Reston, VA, 2012. ISBN: 978-1-60086-894-8.

[2] Yuan, L. C.-L., "Homing and navigational courses of automatic target-seeking devices," *Journal of Applied Physics*, Vol. 19, No. 12, 1948, pp. 1122–1128. https://doi.org/doi.org/10.1063/1.1715028.

[3] Bennett, R., and Mathews, W., "Analytical determination of miss distances for linear homing navigation systems," *Hughes Aircraft Company Technical Memorandum*, , No. 260, 1952.

[4] Murtaugh, S. A., and Criel, H. E., "Fundamentals of proportional navigation," *IEEE spectrum*, Vol. 3, No. 12, 1966, pp. 75–85. https://doi.org/10.1109/MSPEC.1966.5217080.

[5] Guelman, M., "A qualitative study of proportional navigation," *IEEE Transactions on Aerospace and Electronic Systems*, , No. 4, 1971, pp. 637–643.

[6] Guelman, M., "Proportional navigation with a maneuvering target," *IEEE Transactions on Aerospace and Electronic Systems*, , No. 3, 1972, pp. 364–371.

[7] Guelman, M., "Missile acceleration in proportional navigation," *IEEE Transactions on Aerospace and Electronic Systems*, , No. 3, 1973, pp. 462–463.

[8] Becker, K., "Closed-form solution of pure proportional navigation," *IEEE Transactions on Aerospace and Electronic Systems*, Vol. 26, No. 3, 1990, pp. 526–533.

[9] Ghawghawe, S., and Ghose, D., "Pure proportional navigation against time-varying target manoeuvres," *IEEE Transactions on Aerospace and Electronic Systems*, Vol. 32, No. 4, 1996, pp. 1336–1347.

[10] Ha, I.-J., Hur, J.-S., Ko, M.-S., and Song, T.-L., "Performance analysis of PNG laws for randomly maneuvering targets," *IEEE Transactions on Aerospace and Electronic Systems*, Vol. 26, No. 5, 1990, pp. 713–721.

[11] Song, S.-h., and Ha, I.-J., "A Lyapunov-like approach to performance analysis of 3-dimensional pure PNG laws," *IEEE Transactions on Aerospace and Electronic Systems*, Vol. 30, No. 1, 1994, pp. 238–248. https://doi.org/10.1109/7.250424.

[12] Oh, J.-H., and Ha, I.-J., "Capturability of the 3-dimensional pure PNG law," *IEEE Transactions on Aerospace and Electronic Systems*, Vol. 35, No. 2, 1999, pp. 491–503. https://doi.org/10.1109/7.766931.

[13] Ghosh, S., Ghose, D., and Raha, S., "Capturability of augmented pure proportional navigation guidance against time-varying target maneuvers," *Journal of Guidance, Control, and Dynamics*, Vol. 37, No. 5, 2014, pp. 1446–1461.

[14] Babu, K. R., Sarma, I., and Swamy, K., "Switched bias proportional navigation for homing guidance against highly maneuvering targets," *Journal of Guidance, Control, and Dynamics*, Vol. 17, No. 6, 1994, pp. 1357–1363. https://doi.org/10.2514/3.21356.

[15] Nesline, F. W., and Zarchan, P., "A new look at classical vs modern homing missile guidance," *Journal of Guidance and Control*, Vol. 4, No. 1, 1981, pp. 78–85. https://doi.org/10.2514/3.56054.

[16] Anderson, G. M., "Comparison of optimal control and differential game intercept missile guidance laws," *Journal of Guidance and Control*, Vol. 4, No. 2, 1981, pp. 109–115. https://doi.org/10.2514/3.56061.

[17] Shinar, J., and Shima, T., "Nonorthodox guidance law development approach for intercepting maneuvering targets," *Journal of Guidance, Control, and Dynamics*, Vol. 25, No. 4, 2002, pp. 658–666. https://doi.org/10.2514/2.4960.

[18] Pastrick, H., Seltzer, S., and Warren, M., "Guidance laws for short-range tactical missiles," *Journal of Guidance and Control*, Vol. 4, No. 2, 1981, pp. 98–108. https://doi.org/10.2514/3.56060.

[19] Vathsal, S., and Sarkar, A., "Current trends in tactical missile guidance," *Defence Science Journal*, Vol. 55, No. 3, 2005, p. 265. https://doi.org/10.14429/dsj.55.1991.

[20] Garnell, P., and East, D. J., *Guided weapon control systems*, Vol. 2, Pergamon press New York, 1980.

[21] Baba, Y., Yamaguchi, M., and Howe, R. M., "Generalized guidance law for collision courses," *Journal of guidance, control, and dynamics*, Vol. 16, No. 3, 1993, pp. 511–516. https://doi.org/10.2514/3.21039.

[22] Baba, Y., Takehira, T., and Takano, H., "New guidance law for a missile with varying velocity," *Guidance, Navigation, and Control Conference*, 1994, p. 3565. https://doi.org/10.2514/6.1994-3565.

[23] Gazit, R., and Gutman, S., "Development of guidance laws for a variable-speed missile," *Dynamics and Control*, Vol. 1, No. 2, 1991, pp. 177–198. https://doi.org/10.1007/BF02169549.

[24] Gazit, R., "Guidance to collision of a variable-speed missile," *Proceedings. The First IEEE Regional Conference on Aerospace Control Systems,*, IEEE, 1993, pp. 734–737. https://doi.org/10.1109/AEROCS.1993.721030.

[25] Gutman, S., *Applied min-max approach to missile guidance and control*, American Institute of Aeronautics and Astronautics, Inc., 2005. ISBN: 978-1-56347-695-2.

[26] Cho, H., Ryoo, C. K., and Tahk, M.-J., "Closed-form optimal guidance law for missiles of time-varying velocity," *Journal of Guidance, Control, and Dynamics*, Vol. 19, No. 5, 1996, pp. 1017–1022. https://doi.org/10.2514/3.21740.

[27] Shima, T., and Shinar, J., "Time-varying linear pursuit-evasion game models with bounded controls," *Journal of Guidance, Control, and Dynamics*, Vol. 25, No. 3, 2002, pp. 425–432. https://doi.org/10.2514/2.4927.

[28] Taub, I., and Shima, T., "Intercept angle missile guidance under time varying acceleration bounds," *Journal of Guidance, Control, and Dynamics*, Vol. 36, No. 3, 2013, pp. 686–699. https://doi.org/10.2514/1.59139.

[29] Reisner, D., and Shima, T., "Optimal guidance-to-collision law for an accelerating exoatmospheric interceptor missile," *Journal of Guidance, Control, and Dynamics*, Vol. 36, No. 6, 2013, pp. 1695–1708. https://doi.org/10.2514/1.61258.

[30] Lu, P., "Intercept of nonmoving targets at arbitrary time-varying velocity," *Journal of guidance, control, and dynamics*, Vol. 21, No. 1, 1998, pp. 176–178. https://doi.org/10.2514/2.4217.

[31] Jung, Y.-S., Lee, J.-I., Lee, C.-H., and Tahk, M.-J., "A new collision control guidance law based on speed control for kill vehicles," *International Journal of Aeronautical and Space Sciences*, Vol. 20, No. 3, 2019, pp. 792–805. https://doi.org/10.1007/s42405-019-00147-8.

[32] Mishley, A., and Shaferman, V., "Optimal Guidance with an Intercept Angle Constraint for Varying Speed Adversaries," *AIAA SCITECH 2022 Forum*, 2022, p. 1598. https://doi.org/10.2514/6.2022-1598.

[33] Mishley, A., and Shaferman, V., "Linear Quadratic Guidance Laws with Intercept Angle Constraints and Varying Speed Adversaries," *Journal of Guidance, Control, and Dynamics*, Vol. 45, No. 11, 2022, pp. 2091–2106.

[34] Li, K.-B., Liu, Y.-H., Liang, Y.-G., and Chen, L., "Performance of PPN Guided Missile with Arbitrary Time-Varying Speed against Stationary Targets: New Findings," *2022 5th International Symposium on Autonomous Systems (ISAS)*, 2022, pp. 1–8. https://doi.org/10.1109/ISAS55863.2022.9757319.

[35] Cho, N., and Lee, Y.-I., "Guidance Synthesis with Separate Impact Point Prediction Considering Speed Variations," *Journal of Guidance, Control, and Dynamics*, Vol. 44, No. 2, 2021, pp. 428–440. https://doi.org/10.2514/1.G005191.

[36] Song, K.-R., Kim, T.-H., Lee, C.-H., and Tahk, M.-J., "A new guidance algorithm against high-speed maneuvering target," *International Journal of Aeronautical and Space Sciences*, 2021, pp. 1–13.

[37] Oh, J.-H., "Solving a nonlinear output regulation problem: zero miss distance of pure PNG," *IEEE transactions on automatic control*, Vol. 47, No. 1, 2002, pp. 169–173.

[38] Qian, S., Huang, S., Song, X., and Zhang, W., "Zero miss distance of 3D PPNG with time-varying speed," *2019 Chinese Control Conference (CCC)*, IEEE, 2019, pp. 4172–4177.

[39] Li, C.-Y., and Jing, W.-X., "Geometric approach to capture analysis of PN guidance law," *Aerospace Science and Technology*, Vol. 12, No. 2, 2008, pp. 177–183.

[40] Paul, N., and Ghose, D., "Longitudinal-Acceleration-Based Guidance Law for Maneuvering Targets Inspired by Hawk's Attack Strategy," *Journal of Guidance, Control, and Dynamics*, 2023, pp. 1–11.

[41] Brighton, C. H., and Taylor, G. K., "Hawks steer attacks using a guidance system tuned for close pursuit of erratically manoeuvring targets," *Nature Communications*, Vol. 10, No. 1, 2019, pp. 1–10.

[42] Royden, H. L., and Fitzpatrick, P., *Real analysis*, Vol. 32, Macmillan New York, 1988.